

ARTICLE

<https://doi.org/10.1038/s42004-019-0251-z>

OPEN

Stacked nanocarbon photosensitizer for efficient blue light excited Eu(III) emission

Yuichi Kitagawa^{1,2*}, Fumiya Suzue¹, Takayuki Nakanishi³, Koji Fushimi¹, Tomohiro Seki¹, Hajime Ito^{1,2} & Yasuchika Hasegawa^{1,2*}

Photosensitizer design to allow effective use of low-energy light is important for developing photofunctional materials. Herein, we describe a rational photosensitizer design for effective use of low-energy light. The developed photosensitizer is a stacked nanocarbon based on a rigid polyaromatic framework, which allows efficient energy transfer from the low-energy T_1 level to the energy acceptor. We prepared an Eu(III) complex consisting of a luminescent center (Eu(III)) and stacked-coronene photosensitizer. The brightness of photosensitized Eu(III) excited using low-energy light (450 nm) is more than five times higher than the maximum brightness of previously reported Eu(III) complexes.

¹ Faculty of Engineering, Hokkaido University, Kita-13, Nishi-8 Sapporo Hokkaido 060-8628, Japan. ² Institute for Chemical Reaction Design and Discovery (WPI-ICReDD), Hokkaido University, Sapporo Hokkaido 001-0021, Japan. ³ Faculty of Industrial Science and Technology, Tokyo University of Science, 6-3-1, Nijuku Katsushika-ku Tokyo 125-8585, Japan. *email: y-kitagawa@eng.hokudai.ac.jp; hasegaway@eng.hokudai.ac.jp

Organic photosensitizers are molecules that efficiently absorb light and then transfer energy to other species. Photosensitizers are attractive for use in photochemical reactions^{1–3}, energy conversion systems^{4–6}, and luminophores^{7–9}. However, finding a photosensitizer design that achieves both highly efficient low-energy light absorption and energy transfer remains a major challenge.

Most reported photofunctional materials with organic photosensitizers contain heavy metal atoms as effective photoactive centers. The photosensitizer undergoes efficient intersystem crossing (ISC) from the lowest singlet excited state (S_1) to the lowest triplet excited state (T_1) after excitation, transferring its electronic energy to an energy acceptor. According to the energy transfer (ET) process involved, the following two effective photosensitizer design strategies have been reported for luminophore photosensitization.

(a) A conventional design strategy uses strong light absorption to induce photosensitizer excitation from the ground state (S_0) to a singlet excited state (S_n) and tuning of an energy-donating (T_1) level to realize effective photosensitized ET (Fig. 1a). Here, a high T_1 level is required to suppress photon loss derived from back ET from the energy-accepting state (EAS) to T_1 . Thus, this strategy includes two energy-loss processes (ISC and ET), which makes it difficult to apply to low-energy excitation.

(b) The other major photosensitization strategy is to use a spin-forbidden transition (S-T transition) to suppress the energy-loss processes (Fig. 1b)^{10–17}. The S-T transition probability can be enhanced by a heavy atom effect. For example, Ward achieved green emission from blue light-sensitized Tb(III) using photosensitizers that contained heavy metals, such as Ir(III) complexes¹⁰. However, this design strategy suffers from the following disadvantages. (i) The increase of S-T transition probability induced by the heavy metal effect is not large enough for the S-T transition probability to reach the spin-allowed transition probability. (ii) The heavy metal effect also increases the transition probability from T_1 to S_0 . The rapid deactivation of T_1 leads to ineffective ET from T_1 to EAS. (iii) A high T_1 level is still required

to suppress photon loss derived from back ET from EAS, making it difficult to use low-energy excitation.

(c) Herein, we present a novel design to achieve photosensitized emission with low-energy excitation (Fig. 1c). The photosensitizer is based on a stacked nanocarbon composed of a large π -conjugated polyaromatic framework. The polycyclic aromatic framework was selected as a photosensitizer component because of its long T_1 lifetime^{18–21}. The long T_1 lifetime is expected to allow the efficient use of photons even in the case of low T_1 level with ET equilibration between EAS and T_1 . A large π -conjugated nanocarbon with high symmetry induces small $\Delta E(S_1-T_1)$ ²², thus resulting in a high ISC yield. In addition, the stacking of the π -conjugated framework²³ further extends the T_1 lifetime and promotes ISC^{24–27}. Thus, the stacked nanocarbon with long-lived photons and small S_1-T_1 and T_1 -EAS energy gaps lead to both strong low-energy light absorption and highly efficient ET.

To demonstrate our concept, we targeted Eu(III) complexes. In Eu(III) complexes, Eu(III) and the organic ligands act as the emission center and photosensitizer, respectively. The emission lifetime of Eu(III) is usually long because it involves a forbidden 4f–4f transition^{28,29}, so we expected Eu(III) to be the most appropriate acceptor to evaluate the validity of our design concept. We chose coronene as the nanocarbon antenna for the Eu(III) complex because its T_1 level is similar to the emission energy of Eu(III). Bidentate phosphine oxide ligands, which contain the coronene framework, are introduced to the Eu(III) complex to form a rigid structure (i.e., nanocarbon ligand **1**, Fig. 2a). The rigidity of ligand **1** was an important structure factor that induced a long T_1 lifetime³⁰. To further increase the rigidity of the nanocarbon ligand, hexafluoroacetylacetonate (hfa) auxiliary ligands were used to induce formation of intramolecular CH–F interactions in the Eu(III) complex (Fig. 2b)³¹.

Results

Coordination structure. A single crystal of the Eu(III) complex was obtained by recrystallization from a CH_2Cl_2 /hexane solution. Single-crystal X-ray analysis revealed the formation of a dinuclear

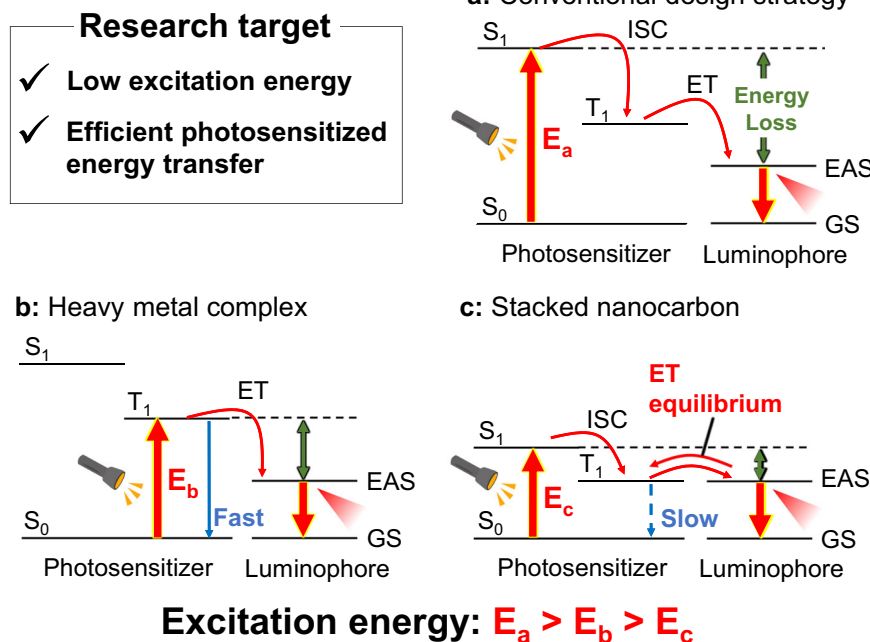


Fig. 1 Photosensitizer design strategies. **a** Conventional design strategy for photosensitized emission (ISC: intersystem crossing, EAS: energy-accepting state, GS: ground state). **b** Heavy metal complex photosensitizer for use of low-energy light. **c** Stacked nanocarbon photosensitizer for use of low-energy light.

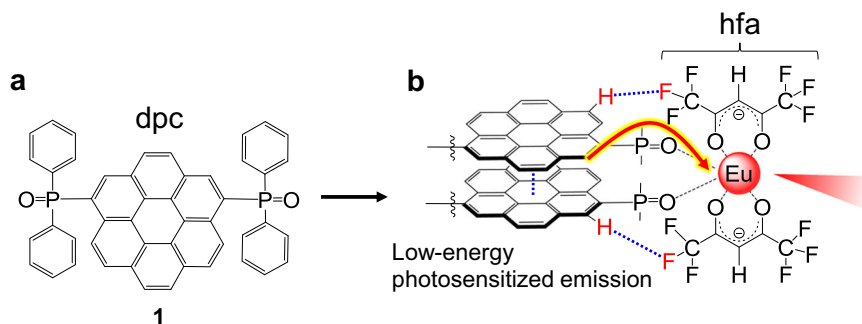


Fig. 2 Molecular structures. **a** Chemical structures of nanocarbon ligand **1**. **b** A schematic image of Eu(III) complex containing **1**.

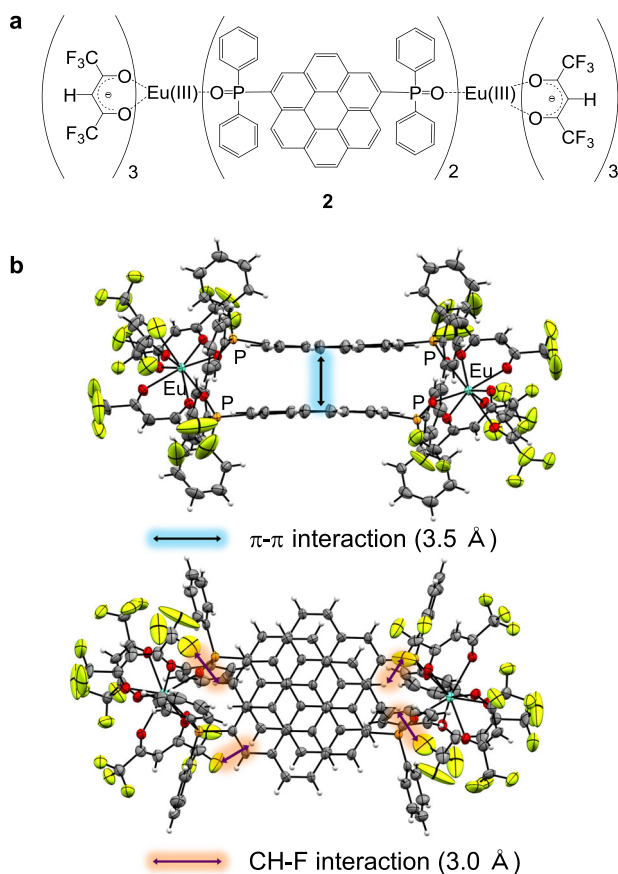


Fig. 3 Stacked nanocarbon structure. **a** Chemical structure (**2**) and **b** ORTEP drawings (ellipsoids probability: 50%) of the Eu(III) complex.

Eu(III) complex (**2**, Fig. 3, Supplementary Table 1). In the dinuclear structure, two Eu(hfa)₃ units are connected by two nanocarbon ligands **1**. The two nanocarbon ligands are located between the Eu(III) centers and form intramolecular π - π interactions (3.5 Å), resulting in H-type exciton (Supplementary Note 1 and Supplementary Fig. 1). A shape measurement calculation³² indicated that the coordination geometry of Eu(III) complex **2** was an asymmetric trigonal dodecahedron (D_{2d}) structure. The stacked nanocarbon ligands **1** are surrounded by hfa ligands, forming effective intramolecular CH-F interactions (3.0 Å). This structure analysis confirmed that the rigid stacked nanocarbon antenna were attached to the Eu(III) centers.

Photophysical properties. The electronic absorption spectrum of Eu(III) complex **2** is shown in Fig. 4. Absorption bands are

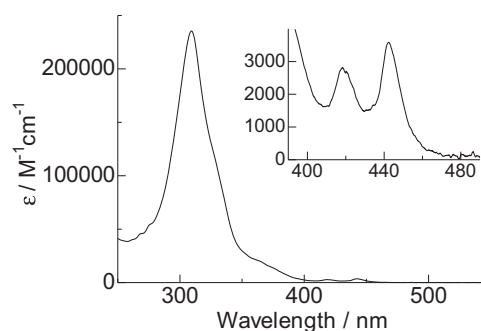


Fig. 4 Electronic absorption spectroscopy. Electronic absorption spectrum of the Eu(III) complex (**2**) in CH₂Cl₂ (3.8×10^{-6} M).

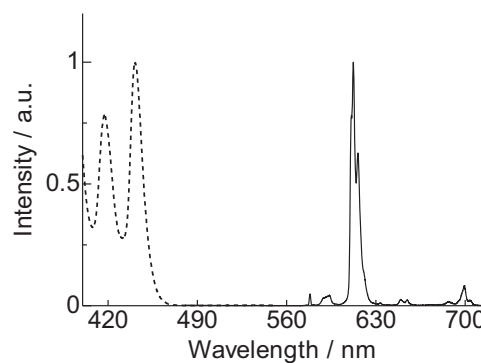


Fig. 5 Emission properties. Emission (black solid line, $\lambda_{\text{ex}} = 450$ nm) and excitation (black broken line, $\lambda_{\text{em}} = 613$ nm) spectra of Eu(III) complex (**2**) in CH₂Cl₂ (3.0×10^{-5} M).

observed at 442 nm ($3600 \text{ M}^{-1} \text{ cm}^{-1}$), 418 nm ($2800 \text{ M}^{-1} \text{ cm}^{-1}$), and 309 nm ($235,400 \text{ M}^{-1} \text{ cm}^{-1}$). These bands originate from π - π^* transitions in the framework of nanocarbon ligand **1**. The weak and strong absorption bands at 442 and 309 nm, respectively, are attributed to the highly symmetric electronic structure with strong configuration interactions (Supplementary Note 2, Supplementary Table 2, and Supplementary Fig. 2). The absorption band at 442 nm is red-shifted from that of the free nanocarbon ligand **1** at 435 nm (Supplementary Note 3 and Supplementary Fig. 3) because of effective charge resonance interactions in complex **2**³³. The electronic interactions induce delocalized S_n in the stacked nanocarbon antenna, yielding extensive absorption areas.

The emission and excitation spectra of complex **2** are presented in Fig. 5 (Supplementary Fig. 4). Emission peaks are observed at 578, 594, 612, 654, and 699 nm, which are assigned to the

$^5D_0 \rightarrow ^7F_0$, $^5D_0 \rightarrow ^7F_1$, $^5D_0 \rightarrow ^7F_2$, $^5D_0 \rightarrow ^7F_3$, and $^5D_0 \rightarrow ^7F_4$ transitions, respectively. Time-resolved emission measurements (Supplementary Note 4 and Supplementary Figs. 5–7) of complex **2** revealed single-exponential decays with lifetimes on the scale of milliseconds (0.7 ms). The rate constants of radiative and non-radiative decay (k_r and k_{nr} , respectively) of complex **2** calculated from the emission lifetime and spectrum³⁴ are 8.8×10^2 and $5.6 \times 10^2 \text{ s}^{-1}$, respectively. The calculated emission quantum yield resulting from excitation of Eu(III) is 61%. The excitation spectrum contains peaks at 442 and 418 nm, which are consistent with peaks observed in the absorption spectrum of nanocarbon **1**, indicating effective ET from ligand **1** to Eu(III) in complex **2**.

The photosensitization properties of Eu(III) complexes fabricated based on the conventional design, heavy metal complex design, and stacked nanocarbon design strategies are compared in Table 1. Strongly luminescent Eu(III) complex **3** excited by UV light (Fig. 6a) was used as a representative molecule designed by the conventional strategy^{35,36}. Luminescent Eu(III) complex **4** (Fig. 6b), which was reported to display the strongest emission when it was excited by 450-nm blue light (the lowest energy light for photosensitized Eu(III) emission)¹¹ was used to represent a material designed according to the S-T transition strategy. The emission efficiency following excitation by nanocarbon ligand **1** (Φ_{tot}) and photosensitization efficiency (η_{sens}) of **2** are estimated to be 36% and 59%, respectively (Supplementary Note 5 and Supplementary Fig. 8). The brightness (I_{total}) of an Ln(III) complex can be written as³⁷

$$I_{\text{total}} = \varepsilon \times \Phi_{\text{tot}} \quad (1)$$

Table 1 Photophysical properties of Eu(III) complexes (Fig. 3a (2), Fig. 6a, b (3–4))^{11,35,36}.

	$a\varepsilon_{\text{max}}$ ($\text{M}^{-1} \text{cm}^{-1}$)	$a\varepsilon_{450}$ ($\text{M}^{-1} \text{cm}^{-1}$)	$b\varepsilon_{\text{tot}}/\%$	ϕ_{max} ($\text{M}^{-1} \text{cm}^{-1}$)	ϕ_{450} ($\text{M}^{-1} \text{cm}^{-1}$)
3 ^{35,36}	25,200	≈ 0	59	1.5×10^4	≈ 0
4 ¹¹	—	600	18	—	1.1×10^2
2	235,400	1700	36	8.5×10^4	6.1×10^2

^aMolar absorption coefficient at absorption maxima (**3**: 306 nm, **2**: 309 nm) and 450 nm. The ε_{450} value of **4** is the molar absorption coefficient of the Ir(III)-based photosensitizer moiety at 451 nm¹¹

^b $\lambda_{\text{ex}} = 370 \text{ nm}$ (**3**), $\lambda_{\text{ex}} = 480 \text{ nm}$ (**4**), $\lambda_{\text{ex}} = 450 \text{ nm}$ (**2**)

^c $\phi_{\text{max}} = \varepsilon_{\text{max}} \times \Phi_{\text{tot}}$, $\phi_{450} = \varepsilon_{450} \times \Phi_{\text{tot}}$. Here, Φ_{tot} is dimensionless

Based on our definition of the photosensitization performance, values of I_{max} ($= \varepsilon_{\text{max}} \times \Phi_{\text{tot}}$) and I_{450} ($= \varepsilon_{450 \text{ nm}} \times \Phi_{\text{tot}}$) estimated for complex **2–4** are listed in Table 1. I_{max} of **2** ($8.5 \times 10^4 \text{ M}^{-1} \text{cm}^{-1}$) exceeds that of the strongly luminescent complex **3** ($1.5 \times 10^4 \text{ M}^{-1} \text{cm}^{-1}$). The brightness of **2** ($6.1 \times 10^2 \text{ M}^{-1} \text{cm}^{-1}$) excited by 450-nm light is five times larger than that of complex **4** ($1.1 \times 10^2 \text{ M}^{-1} \text{cm}^{-1}$), which is the Eu(III) complex with the strongest emission under 450-nm excitation reported until now (Supplementary Note 6)¹¹. These results demonstrate that the stacked nanocarbon ligands induce excellent photosensitized emission properties in **2**.

Mechanistic study. To confirm the mechanism of the extremely high I_{450} of **2**, the phosphorescence spectrum of Gd(III) complex **5** (Fig. 7) in 2-methyltetrahydrofuran ($6.0 \times 10^{-5} \text{ M}$) was measured to estimate T_1 of the stacked nanocarbon ligands **1** (Fig. 8). The estimated T_1 level ($18,900 \text{ cm}^{-1}$) yielded a smaller $\Delta E(S_1-T_1)$ (3700 cm^{-1}) than those of typical organic compounds (ex. Eu(III) complex **3**^{35,36}, anthracene³⁸, and a phthalocyanine derivative³⁹ are 11,100, 11,700, and ca. 5000 cm^{-1} , respectively) (Supplementary Fig. 9). The EAS of Eu(III) that accepts energy from the stacked nanocarbon ($T_1 = 18,900 \text{ cm}^{-1}$) in **2** corresponds to the 5D_0 level ($17,250 \text{ cm}^{-1}$) in contrast to existence of the several EAS (5D_0 , 5D_1 : 19,100 cm^{-1} , 5D_2 : 21,400 cm^{-1}) of Eu(III) complexes **3** ($T_1 = 21,700 \text{ cm}^{-1}$, Supplementary Note 7 and Supplementary Fig. 10)⁴⁰ and **4** ($T_1 = 21,300 \text{ cm}^{-1}$)¹¹. Although a direct energy transfer to the 5D_0 level is not allowed⁴¹, the energy transfer from T_1 to 5D_0 in the Eu(III) complex can be induced by the J-mixing effects and thermal population of the 7F_1 level. The energy gap between the photosensitizer and energy acceptor (1650 cm^{-1}) induces strong back ET from 5D_0 to T_1 in **2**^{42,43}.

To clarify the efficient energy migration mechanism with back ET, the time-resolved emission profile of Gd(III) complex **5** was also measured (Fig. 9, black solid line). The estimated T_1 lifetime was 6.2 s, which is 1000 times longer than those of previously reported efficient photosensitized antennas designed by conventional strategy (Fig. 9, red solid line)⁴⁰. The long T_1 lifetime at 100 K is considered to be based on the small radiative rate constant originating from a small spin-orbit coupling. We estimated the T_1 lifetime of **5** at 300 K using the Arrhenius plots of temperature-dependent emission lifetime (Supplementary Note 8 and Supplementary Fig. 11)⁴⁴. The estimated T_1 lifetime is 40 ms, which is about 50 times longer than Eu(III) emission lifetime. This long lifetime caused by the stacked nanocarbon ligands allows efficient ET from the nanocarbon ligands to Eu(III) ($T_1 \rightarrow ^5D_0$) and strong population of the emitting 5D_0 level from

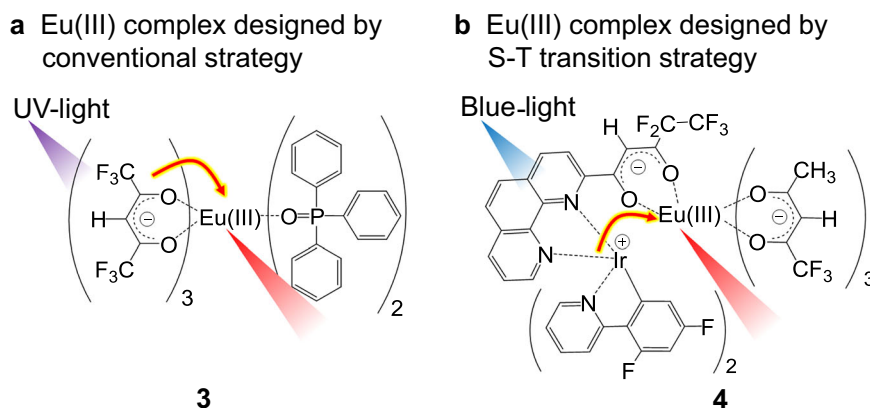


Fig. 6 Previously reported Eu(III) complexes. a Eu complex **3** with UV light-sensitized emission based on the conventional design strategy (Fig. 1a)^{35,36}. **b** Eu complex **4** with blue light-sensitized emission based on the S-T transition strategy (Fig. 1b)¹¹.

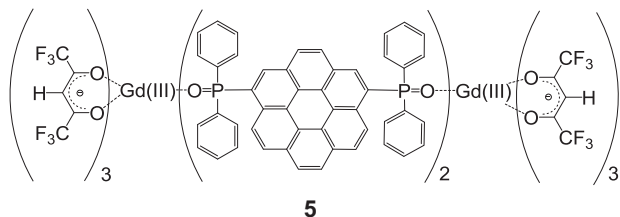


Fig. 7 Structure of (5). Chemical structure of Gd(III) complex (5).

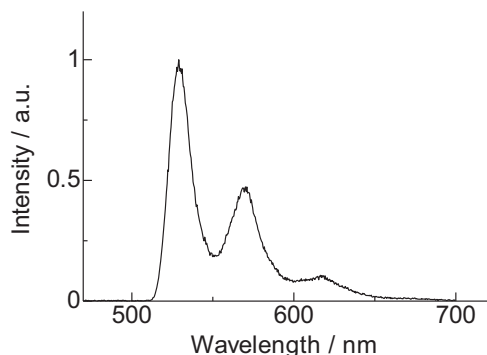


Fig. 8 Phosphorescence spectroscopy. Phosphorescence spectrum of Gd(III) complex (5) (90 K, delay: 50 ms, 2Me-THF: 6.0×10^{-5} M, $\lambda_{\text{ex}} = 420$ nm).

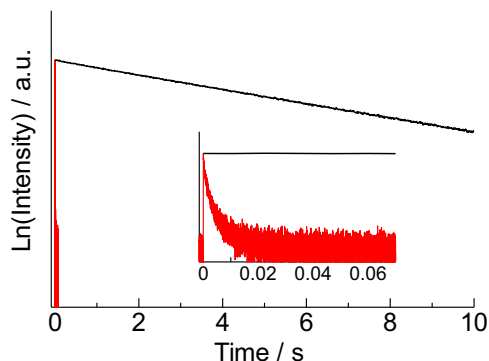


Fig. 9 Time-resolved emission intensities. Phosphorescence decays of Gd(III) complex (5) (black solid line, 100 K, delay: 50 ms, 2Me-THF: 6.0×10^{-5} M, $\lambda_{\text{ex}} = 420$ nm) and previous Gd(III) complex with the same ligands of 3 (red solid line, 100 K, delay: 0 ms, solid state, $\lambda_{\text{ex}} = 355$ nm)⁴⁰.

the low-lying T_1 level. In contrast to our strategy, since the lifetime of Eu(III) complex (4) is short enough (24 μs), a high T_1 level is required to suppress the photon loss derived from back ET from EAS (Fig. 1b).

The small $\Delta E(S_1-T_1)$ is also important for both low-energy light absorption and efficient energy migration (Fig. 1c). The light-absorbing energy level $E(S_1)$ can be expressed as:

$$E(S_1) = E(T_1) + 2K_{if} \quad (2)$$

where K is an exchange integral between orbital pairs and subscripts i and f are the occupied and unoccupied orbitals related to S_1 , respectively. Molecules with extended π -conjugation show small $\Delta E(S_1-T_1)$ because of the small K_{if} ²⁴. The efficient ET from the low $E(T_1)$ and small $2K_{if}$ enable efficient emission from 2 under low-energy light irradiation. The previously reported Eu(III) complex with high I_{450} (4) uses the S-T transition involving

the heavy atomic effect (Fig. 1b) to achieve an extensive absorption area. In contrast, we developed a novel design concept based on a metal-free stacked nanocarbon ligand 1 for the achievement of small $\Delta E(S_1-T_1)$ and $\Delta E(T_1-EAS)$. This strategy achieves not only an extensive absorption area but also efficient energy migration to realize a high-performance photosensitizer.

In this study, we proposed a stacked nanocarbon photosensitizer to enhance photosensitized emission efficiency. Based on the design strategy, we demonstrated that the brightness of the Eu(III) complex 2 with stacked-coronene photosensitizers exhibited $6.1 \times 10^2 \text{ M}^{-1} \text{ cm}^{-1}$ when excited by blue light, which is five times higher than the maximum brightness of a previously reported Eu(III) complex excited by 450-nm light ($1.1 \times 10^2 \text{ M}^{-1} \text{ cm}^{-1}$)¹¹. This study provides insights for the photosensitizer design in order to develop photofunctional materials that utilize low-energy light.

Methods

General method. ¹H-NMR spectra were recorded in CDCl_3 on a JEOL ECS-400 (400 MHz) spectrometer; tetramethylsilane was used as the internal reference. Electron ionization (EI) and electrospray ionization (ESI) mass spectrometry were performed using JEOL JMS-T100 GCv and JEOL JMS-T100 LP instruments, respectively. Elemental analyses were performed using MICRO CORDER JM10. UV-vis absorption spectra for ligand 1 and Eu(III) complex 2 were measured using a JASCO V-670 spectrophotometer. Emission spectrum, excitation spectrum, and emission lifetime for Eu(III) complex 2 were measured using a Horiba FluoroLog[®]3 spectrofluorometer. Emission spectrum and lifetime for Gd(III) complex 5 were measured using a FP-6300 spectrofluorometer with a nitrogen bath cryostat (Oxford Instruments, Optistat DN) and a temperature controller (Oxford Instruments ITC-502S). Emission spectrum for the ligand 1 was measured using a FP-6300 spectrofluorometer with a nitrogen bath cryostat (Oxford Instruments, Optistat DN) and a temperature controller (Oxford Instruments ITC-502S). Emission quantum yield for Eu(III) complex 2 was measured using a FP-6300 spectrofluorometer with an integration sphere (ILF-533).

Preparation of ligand 1. A solution of *n*-butyllithium (*n*-BuLi, 2.0 mL, 3.14 mmol) was added dropwise to a suspension of 1,6-dibromo-coronene (530 mg, 1.16 mmol) in dry THF (150 mL) at -80°C under Ar. After cooling for 30 min, chlorodiphenylphosphine (0.5 mL, 2.71 mmol) was added to the suspension, which was then stirred for 7 h at room temperature. The product was evaporated and extracted using dichloromethane; the extract was washed with distilled water and then dried over anhydrous MgSO_4 . The solution was cooled and a 30% H_2O_2 aqueous solution (2 mL) was added. The reaction mixture was stirred for 3 h. The product was again extracted using dichloromethane; the extract was washed with distilled water and then dried over anhydrous MgSO_4 . The compounds were separated by silica gel chromatography with ethyl acetate as the mobile phase. The solvent was evaporated to yield a yellow powder (Fig. 2a).

ESI-MS: m/z calcd for $\text{C}_{48}\text{H}_{31}\text{O}_2\text{P}_2$ [$\text{M} + \text{H}$]⁺ = 701.18; found: 701.18.

IR (ATR): 3052 (st, C-H), 1182 (st, P=O) cm^{-1} .

¹H-NMR (400 MHz, CDCl_3): δ /ppm = 7.45–7.66 (m, 12H), 7.79–7.94 (m, 8H), 8.59–8.96 (m, 8H), 9.61–9.69 (q, 1H), 9.71–9.77 (t, 1H).

Preparation of Eu(III) complex 2. Dichloromethane (30 mL) containing Eu(hfa)₃(H₂O)₂ (300 mg, 0.37 mmol) and ligand 1 (175 mg, 0.25 mmol) was refluxed under stirring for 2 h at 40°C . The reaction mixture was filtrated, and the filtrate was concentrated using a rotary evaporator. Recrystallization from CH_2Cl_2 /hexane solution gave yellow crystals (Yield: 3%, 25 mg, Fig. 3a).

ESI-MS: m/z calcd for $\text{C}_{121}\text{H}_{65}\text{Eu}_2\text{F}_{30}\text{O}_{14}\text{P}_4$ [M-hfa]⁺ = 2741.13; found: 2741.17.

Elemental analysis (%): calcd for $\text{C}_{126}\text{H}_{66}\text{Eu}_2\text{F}_{36}\text{O}_{16}\text{P}_4$: C 51.34, H 2.26; found: C 51.46, H 2.22.

IR (ATR): 1143 (st, P=O), 1251 (st, C-F), 1652 (st, C=O), 3061 (st, arC-H) cm^{-1} .

Further information on the materials and preparation is given in the Supplementary Methods section.

Single-crystal X-ray structure determination. X-ray crystal structures and crystallographic data for Eu(III) complex 2 is shown in Fig. 3b and Table S1. Single crystals of the compounds were mounted on micromesh (MiTeGen M3-L19-25L) using paraffin oil. Measurements were made by using a Rigaku RAXIS RAPID imaging-plate area detector or XtaLAB AFC11 (RCD3) with graphite-monochromated Mo-K α radiation. Non-hydrogen atoms were anisotropically refined. All calculations were performed using a crystal-structure crystallographic software package. The CIF data were confirmed by the check CIF/PLATON service. CCDC-1885659 (for Eu(III) complex 2) contain the supplementary

crystallographic data for this paper. These data can be obtained free of charge from The Cambridge Crystallographic Data Centre via www.ccdc.cam.ac.uk/data_request/cif.

Calculation of emission quantum yield. The emission quantum yields excited by Eu(III) ion (Φ_{ff}) and the radiative (k_r) and non-radiative (k_{nr}) rate constants were estimated using equations as follows^{34–36}.

$$\tau_{\text{rad}} = \frac{1}{k_r} \quad (3)$$

$$\tau_{\text{obs}} = \frac{1}{k_r + k_{\text{nr}}} \quad (4)$$

$$\Phi_{\text{ff}} = \frac{k_r}{k_r + k_{\text{nr}}} = \frac{\tau_{\text{obs}}}{\tau_{\text{rad}}} \quad (5)$$

$$k_r = A_{\text{MD},0} n^3 \left(\frac{I_{\text{tot}}}{I_{\text{MD}}} \right) \quad (6)$$

$$k_{\text{nr}} = \frac{1}{\tau_{\text{obs}}} - \frac{1}{\tau_{\text{rad}}} \quad (7)$$

where $A_{\text{MD},0}$ is the spontaneous luminescence probability for the ${}^5\text{D}_0 \rightarrow {}^7\text{F}_1$ transition in vacuo (14.65 s^{-1}), n is the refractive index of the medium (1.5), and $(I_{\text{tot}}/I_{\text{MD}})$ is the ratio of the total area of the Eu(III) luminescence spectrum to the area of the ${}^5\text{D}_0 \rightarrow {}^7\text{F}_1$ transition band.

Data availability

The authors declare that the data supporting the findings of this study are available within the paper and its supplementary information. Data for the crystal structures reported in this paper have been deposited at the Cambridge Crystallographic Data Centre (CCDC) under the deposition numbers CCDC-1885659 (2).

Received: 21 August 2019; Accepted: 12 December 2019;

Published online: 03 January 2020

References

- Ravetz, B. D. et al. Photoredox catalysis using infrared light via triplet fusion upconversion. *Nature* **565**, 343–346 (2019).
- Tsuji, Y., Yamamoto, K., Yamauchi, K. & Sakai, K. Near-infrared light-driven hydrogen evolution from water using a polypyridyl triruthenium photosensitizer. *Angew. Chem. Int. Ed.* **57**, 208–212 (2018).
- Liu, Y., Meng, X. & Bu, W. Upconversion-based photodynamic cancer therapy. *Coord. Chem. Rev.* **379**, 82–98 (2019).
- Yang, M.-Q., Gao, M., Hong, M. & Ho, G. W. Visible-to-NIR photon harvesting: progressive engineering of catalysts for solar-powered environmental purification and fuel production. *Adv. Mater.* **30**, 1802894 (2018).
- Li, D., Ågren, H. & Chen, G. Near infrared harvesting dye-sensitized solar cells enabled by rare-earth upconversion materials. *Dalton Trans.* **47**, 8526–8537 (2018).
- Lee, C. P. et al. Recent progress in organic sensitizers for dye-sensitized solar cells. *RSC Adv.* **5**, 23810–23825 (2015).
- Aboshyan-Sorgho, L. et al. Near-infrared \rightarrow visible light upconversion in a molecular trinuclear d-f-d complex. *Angew. Chem. Int. Ed.* **50**, 4108–4122 (2011).
- Koizuka, T. et al. Red luminescent Eu(III) coordination bricks excited on blue LED chip. *Inorg. Chem.* **57**, 7097–7103 (2018).
- Souri, N. et al. Upconverted photosensitization of Tb visible emission by NIR Yb excitation in discrete supramolecular heteropolynuclear complexes. *J. Am. Chem. Soc.* **139**, 1456–1459 (2017).
- Sykes, D. & Ward, M. D. Visible-light sensitisation of Tb(III) luminescence using a blue-emitting Ir(III) complex as energy-donor. *Chem. Commun.* **47**, 2279–2281 (2011).
- Chen, F. F. et al. Highly efficient sensitized red emission from europium (III) in Ir-Eu bimetallic complexes by ${}^3\text{MLCT}$ energy transfer. *Inorg. Chem.* **47**, 2507–2513 (2008).
- Yamazaki, Y. & Ishitani, O. Synthesis of Os(II)–Re(I)–Ru(II) hetero-trinuclear complexes and their photophysical properties and photocatalytic abilities. *Chem. Sci.* **9**, 1031–1041 (2018).
- Kinoshita, T. et al. Enhancement of near-IR photoelectric conversion in dye-sensitized solar cells using an osmium sensitizer with strong spin-forbidden transition. *J. Phys. Chem. Lett.* **3**, 394–398 (2012).
- Kinoshita, T., Dy, J. T., Uchida, S., Kubo, T. & Segawa, H. Wideband dye-sensitized solar cells employing a phosphine-coordinated ruthenium sensitizer. *Nat. Photon.* **7**, 535–539 (2013).
- Kinoshita, T. et al. Spectral splitting photovoltaics using perovskite and wideband dye-sensitized solar cells. *Nat. Commun.* **6**, 8834 (2015).
- Amemori, S., Sasaki, Y., Yanai, N. & Kimizuka, N. Near-infrared-to-visible photon upconversion sensitized by a metal complex with spin-forbidden yet strong $\text{S}_0\text{--T}_1$ absorption. *J. Am. Chem. Soc.* **138**, 8702–8705 (2016).
- Sasaki, Y., Amemori, S., Kouno, H., Yanai, N. & Kimizuka, N. Near infrared-to-blue photon upconversion by exploiting direct S–T absorption of a molecular sensitizer. *J. Mater. Chem. C.* **5**, 5063–5067 (2017).
- Bünzli, J.-C. G. On the design of highly luminescent lanthanide complexes. *Coord. Chem. Rev.* **293–294**, 19–47 (2015).
- Binnemans, K. Interpretation of europium(III) spectra. *Coord. Chem. Rev.* **295**, 1–45 (2015).
- Salinas-Castillo, A., Segura-Carretero, A., Costa-Fernández, J. M., Wei, J. J. & Fernández-Gutiérrez, A. Heavy atom induced room temperature phosphorescence: a tool for the analytical characterization of polycyclic aromatic hydrocarbons. *Anal. Chim. Acta* **516**, 213–220 (2004).
- Offen, H. W. & Hein, D. E. Environmental effects on phosphorescence. VI. Matrix site effects for triphenylene. *J. Chem. Phys.* **50**, 5274–5278 (1969).
- Kropp, J. L. & Dawson, W. R. Radiationless deactivation of triplet coronene in plastics. *J. Phys. Chem.* **71**, 4499–4506 (1967).
- Fetzer, J. C., Zander, M. & Naturforsch, Z. Fluorescence, phosphorescence, and E-type delayed fluorescence of hexabenzobenzene [b, c, d, e, f, g, h, i, j, k, l, m, n, o, p, q, r] coronene. *Z. Naturforsch.* **45**, 727–729 (1990).
- Köhler, A. & Beljonne, D. The singlet–triplet exchange energy in conjugated polymers. *Adv. Funct. Mater.* **14**, 11–18 (2004).
- Silva, N. J., Machado, F. B., Lischka, H. & Aquino, A. J. p-p stacking between polyaromatic hydrocarbon sheets beyond dispersion interactions. *Phys. Chem. Chem. Phys.* **18**, 22300–22310 (2016).
- An, Z. et al. Stabilizing triplet excited states for ultralong organic phosphorescence. *Nat. Mater.* **14**, 685–690 (2015).
- Gu, L. et al. Prolonging the lifetime of ultralong organic phosphorescence through dihydrogen bonding. *J. Mater. Chem. C.* **6**, 226–233 (2018).
- Lucenti, E. et al. H-Aggregates granting crystallization-induced emissive behavior and ultralong phosphorescence from a pure organic molecule. *J. Phys. Chem. Lett.* **8**, 1894–1898 (2017).
- Cai, S. et al. Hydrogen-bonded organic aromatic frameworks for ultralong phosphorescence by intralayer $\pi\text{--}\pi$ interactions. *Angew. Chem. Int. Ed.* **57**, 4005–4009 (2018).
- Mieno, H., Kabe, R., Notsuka, N., Allendorf, M. D. & Adachi, C. Long-lived room-temperature phosphorescence of coronene in zeolitic imidazolate framework ZIF-8. *Adv. Opt. Mater.* **4**, 1015–1021 (2016).
- Miyata, K. et al. Thermostable organo-phosphor: low-vibrational coordination polymers that exhibit different intermolecular interactions. *ChemPlusChem* **77**, 277–280 (2012).
- Casanova, D., Llundell, M., Alemany, P. & Alvarez, S. The rich stereochemistry of eight-vertex polyhedra: a continuous shape measures study. *Chem. Eur. J.* **11**, 1479–1494 (2005).
- Hestand, N. J. & Spano, F. C. Molecular aggregate photophysics beyond the Kasha model: novel design principles for organic materials. *Acc. Chem. Res.* **50**, 341–350 (2017).
- Werts, M. H. V., Jukes, R. T. F. & Verhoeven, J. W. The emission spectrum and the radiative lifetime of Eu^{3+} in luminescent lanthanide complexes. *Phys. Chem. Chem. Phys.* **4**, 1542–1548 (2002).
- Hasegawa, Y. et al. Luminescent polymer containing the Eu(III) complex having fast radiation rate and high emission quantum efficiency. *J. Phys. Chem. A* **107**, 1697–1702 (2003).
- Kitagawa, Y., Suzue, F., Nakanishi, T., Fushimi, K. & Hasegawa, Y. A highly luminescent Eu(III) complex based on an electronically isolated aromatic ring system with ultralong lifetime. *Dalton Trans.* **47**, 7327–7332 (2018).
- Gschneidner, K. A., Bünzli, J.-C. G. & Pecharsky, V. K. *Handbook on the Physics and Chemistry of Rare Earths*, vol. 37 (Elsevier, New York, 2007).
- Nijegorodov, N., Ramachandran, V. & Winkoun, D. P. The dependence of the absorption and fluorescence parameters, the intersystem crossing and internal conversion rate constants on the number of rings in polyacene molecules. *Spectrochim. Acta A* **53**, 1813–1824 (1997).
- Vincett, P. S., Voigt, E. M. & Rieckhoff, K. E. Phosphorescence and fluorescence of phthalocyanines. *J. Chem. Phys.* **55**, 4131–4140 (1971).
- Yamamoto, M., Kitagawa, Y., Nakanishi, T., Fushimi, K. & Hasegawa, Y. Ligand-assisted back energy transfer in luminescent Tb(III) complexes for thermo-sensing properties. *Chem. Eur. J.* **24**, 17719–17726 (2018).
- de Sa, G. F. et al. Spectroscopic properties and design of highly luminescent lanthanide coordination complexes. *Coord. Chem. Rev.* **196**, 165–195 (2000).
- Shi, M. et al. Tuning the triplet energy levels of pyrazolone ligands to match the ${}^5\text{D}_0$ level of europium(III). *Inorg. Chem.* **44**, 8929–8936 (2005).

43. Latva, M. et al. Correlation between the lowest triplet state energy level of the ligand and lanthanide(III) luminescence quantum yield. *J. Lumin.* **75**, 149–169 (1997).
44. Monti, S., Orlandi, G., Kellmann, A. & Tfibel, F. Temperature dependence of the phosphorescence lifetime of nitrobenzopyrans: the role of the lowest triplet state in the reaction of pyran ring opening. *J. Photochem.* **33**, 81–87 (1986).

Acknowledgements

This work was supported by Grant-in-Aid for Grant Number 17K14467, 19H04556, 18H04497, and 18H02041. This work was also supported by the Institute for Chemical Reaction Design and Discovery (ICReDD), established by the World Premier International Research Initiative (WPI) of MEXT, Japan.

Author contributions

Y.K. designed research. F.S. performed syntheses. F.S. and Y.K. performed optical measurements. T.S. and H.I. supported X-ray crystal measurements. Y.K., Y.H., T.N., K.F., T.S., H.I. wrote the paper. All authors reviewed the paper.

Competing interests

The authors declare no competing interests.

Additional information

Supplementary information is available for this paper at <https://doi.org/10.1038/s42004-019-0251-z>.

Correspondence and requests for materials should be addressed to Y.K. or Y.H.

Reprints and permission information is available at <http://www.nature.com/reprints>

Publisher's note Springer Nature remains neutral with regard to jurisdictional claims in published maps and institutional affiliations.



Open Access This article is licensed under a Creative Commons Attribution 4.0 International License, which permits use, sharing, adaptation, distribution and reproduction in any medium or format, as long as you give appropriate credit to the original author(s) and the source, provide a link to the Creative Commons license, and indicate if changes were made. The images or other third party material in this article are included in the article's Creative Commons license, unless indicated otherwise in a credit line to the material. If material is not included in the article's Creative Commons license and your intended use is not permitted by statutory regulation or exceeds the permitted use, you will need to obtain permission directly from the copyright holder. To view a copy of this license, visit <http://creativecommons.org/licenses/by/4.0/>.

© The Author(s) 2020